Journal of Colloid and Interface Science 532 (2018) 464–473

Contents lists available at ScienceDirect

Journal of Colloid and Interface Science

journal homepage: www.elsevier.com/locate/jcis

Regular Article

Multifunctional Ag nanoparticle decorated Si nanowires for sensing, photocatalysis and light emission applications

Ramesh Ghosh [a,b,c], Joydip Ghosh [a], Ruma Das [a], Larionette P.L. Mawlong [b], Kamal Kumar Paul [a], P.K. Giri [a,b,*]

[a] Department of Physics, Indian Institute of Technology Guwahati, Guwahati 781039, India
[b] Centre for Nanotechnology, Indian Institute of Technology Guwahati, Guwahati 781039, India
[c] Department of Physics and Astronomy, Seoul National University, Seoul 151747, Republic of Korea

HIGHLIGHTS

- Ag nanoparticle decorated Si nanowires (Ag@Si NWs) are fabricated by a simple chemical process.
- The Ag@Si NWs show white light emission, ultralow reflectance and high photocatalytic efficiency.
- The Ag@Si NWs exhibit excellent SERS sensitivity with detection limit down to 1 pM.
- The Ag@Si NWs show excellent fluorescence detection sensitivity down to 10 pM level.

GRAPHICAL ABSTRACT

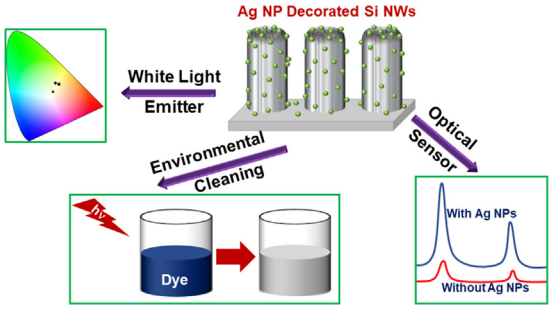

ARTICLE INFO

Article history:
Received 30 March 2018
Revised 25 July 2018
Accepted 28 July 2018
Available online 29 July 2018

Keywords:
Si nanowires
Ag nanoparticles
Photoluminescence
Photocatalysis
SERS
Chemical sensing

ABSTRACT

We report on the fabrication of Ag nanoparticle (NP) decorated mesoporous Si nanowire (NW) heterostructure (HS) by a simple and low cost chemical process. The as-grown Si NWs are mesoporous in nature and the Ag NP decorated Si NWs (Ag@Si NWs) exhibit broadband light emission, ultralow reflectance, efficient photocatalytic degradation of organic dyes and excellent sensitivity for the detection of organic molecules over a wide range of concentration. The broadband white light photoluminescence emission from the bare Si NWs is explained on the basis of quantum confinement effect in Si NCs/NWs and the nonbridging oxygen hole center defects in the Si—SiO_x interface. High work function of the noble metal NPs facilitates the effective separation of the photoinduced electron-hole pairs in Si NWs, which enables the Ag@Si NWs to exhibit high photocatalytic efficiency for the degradation of organic dye. The Ag@Si NWs exhibited high potential and sensitivity for the selective and quantitative detection of different organic molecules at extremely low concentration down to 10^{-12} M by surface-enhanced Raman scattering and 10^{-11} M by fluorescence-based detection. These versatile properties of the Ag@Si NWs open up opportunities for a variety of energy and environmental applications, such as white light emission, solar cell, artificial photosynthesis, disposal of organic pollutant and bio-chemical sensors etc.

1. Introduction

During the past decades, Si nanostructures, including nanoparticles (NPs), nanowires (NWs), nanorods (NRs), nanotubes, nanofibers and nanobelts, have been attracting a great deal of attention in both basic scientific research and potential technological applications due to their fascinating physical and

* Corresponding author at: Department of Physics, Indian Institute of Technology Guwahati, Guwahati 781039, India.
E-mail address: giri@iitg.ernet.in (P.K. Giri).

https://doi.org/10.1016/j.jcis.2018.07.123
0021-9797/

chemical characteristics [1–11]. By incorporating additional complexities and functionalities through the heterostructure (HS) approach, it is possible to modify/improve the selective properties of the Si nanostructures according to the requirements. The unique and enhanced properties of the Si nanostructures, especially Si NWs by forming HSs open up opportunities for various technological applications, such as photovoltaics, artificial photosynthesis, sensors, environmental cleaning, and micro- to nano-electronic devices etc [1–7,12–20]. Among different HSs, metal NP decorated HSs have drawn enormous attention from the application point of view [18,21–29]. For example, noble metals with high work function on Si NWs can facilitate the effective separation of the photoinduced electron-hole pairs and enables the HS to show excellent photocatalytic property [18,21–28]. Metallic NPs for plasmonics have been investigated for various applications, including bio-chemical, gas sensing, photonics, solar cells and photocatalysis. Recent studies demonstrate that metal NPs decorated Si NWs-based nanohybrids exhibit remarkable enhancement in the above-mentioned properties as compared to the free metallic NPs or HSs with other semiconductors. In this context, different metals, e.g. Au, Ag, Pt, Cu, Pd, Ni and Al etc. are used and studied in detail [12–18,21–28]. In some cases, the metal NPs were loaded on Si NW- surface by an electroless deposition technique using a chemical solution. A variety of metal NPs, such as Ag, Au, Pt, Pd, Cu, Co have been decorated on Si NWs by dipping the Si NWs into a solution containing HF and $AgNO_3$, $HAuCl_4$, H_2PtCl_6, $PdAc_2$, $Cu(NO_3)_2$, $Co(NO_3)_2$, respectively [18]. Thermal evaporation techniques have also been utilized to decorate the metal NPs on the Si NWs [12]. Interestingly, bimetal NPs, such as Au—Pd, Pd—Ni are also used to decorate the Si NWs and the HSs exhibited superior properties as compared to that of single metal NP case. Sometimes, the NPs are coated on the radial and branched HSs of Si NWs in order to improve the device performance [13,14]. Among different metals, Ag is one of the most effective materials for the fabrication of multifunctional Si NW HSs [21,26,30]. The fabrication of Ag@Si NWs by an easy, cost effective and efficient process and its utilization in various areas of nanotechnology are very attractive nowadays.

In this work, we have studied the Ag NP decorated mesoporous Si NWs grown by a chemical method using HF and $AgNO_3$ solution. The mesoporous Si NWs were grown by typical metal assisted chemical etching (MACE) process using Ag as the noble metal catalyst and HF/H_2O_2 as the etchant [8–11]. We observe a strong influence of the decorated Ag NPs on the PL and the photocatalytic activity of the Si NW arrays. The Ag@Si NWs shows a broadband white light emission (~1.4–3.0 eV) and its origin was investigated. Furthermore, the high work function of Ag NPs decorated on the Si NWs has resulted in enhanced photocatalytic activity as compared to the bare Si NWs and origin of the same is examined in details. A systematic comparison of the PL and photocatalytic efficiencies of the Si NWs coated with different noble metal NPs was carried out. We have also studied the sensing properties of the Ag@Si NWs as a surface enhanced Raman scattering (SERS) effective substrate for the selective and sensitive detection of Methylene Blue (MB) and Rose Bengal (RB) dyes. The sensing properties of these HSs have also been examined by fluorescence-based detection of MB and Rhodamine B (RhB) at extremely low concentrations.

2. Experimental details

2.1. Fabrication of Si nanowires

Si NWs were grown from p-type and *n*-type Si(1 0 0) wafers with resistivity 0.01 Ω cm. A typical two-step MACE process was used to grow the aligned Si NWs using Ag as the noble metal catalyst and HF/H_2O_2 as the etchant. In this process, first a thin layer of Ag nanoparticles (NPs) was deposited on the Si wafers by dipping it in a solution containing 5.55 M HF and 0.015 M $AgNO_3$ for 5 sec. Next, the as-deposited substrates were immersed in a solution containing 5 ml HF (48%), 2 ml H_2O_2 (50%) and 23 ml DI water for 10 min at room temperature (RT) [8–11,31,32]. The as-grown Si NWs are mesoporous in nature due to the sidewall etching. The residual Ag particles after etching are removed by immersing the as-grown samples into diluted HNO_3 (10%) solution.

Table 1
Details of the growth conditions for different samples with code names.

Sample Code	Sample Specification	Fabrication Process	Time
NW	Si NWs from p-type Si wafer	MACE of Si wafer in 5 ml HF (48%), 2 ml H_2O_2 (50%) and 23 ml DI water	10 min
NW2	Si NWs from *n*-type Si wafer		
NWAg1	Ag NPs decorated on Si NWs	Immersion of the Si NWs into 0.015 M $AgNO_3$ and 5.55 M HF	2 sec
NWAg2			4 sec
NWAg3			6 sec
NWAg4			8 sec
SiAg1	Ag NPs decoration on Si wafer	Immersion of the Si wafers into 0.015 M $AgNO_3$ and 5.55 M HF	2 sec
SiAg2			4 sec
SiAg3			6 sec

2.2. Ag nanoparticle decoration on Si nanowires

Ag NPs are decorated on the surface of the Si NWs by immersing the Si NWs in a solution containing 0.015 M $AgNO_3$ and 5.55 M HF for different durations (a few seconds only). A film of Ag NPs on bulk Si wafer was also prepared by the same process. The details of the sample specifications and corresponding sample codes are provided in Table 1.

2.3. Characterization techniques

The morphology and the structure of the Si NWs and its HSs were characterized using a field emission scanning electron microscope (FESEM) (Sigma, Zeiss). The high magnification surface morphologies of Ag@Si NWs were studied using a transmission electron microscope (TEM) (JEOL-JEM 2010) operated at 200 kV. For the compositional analysis, X-ray photoelectron spectroscopy (XPS) measurements were carried out using a PHI X-Tool automated photoelectron spectrometer (ULVAC-PHI Inc.) using Al Kα X-ray beam (1486.6 eV) with a beam current of 20 mA. Carbon 1 spectrum was used for the calibration (284.8 eV) of the XPS spectra recorded for various samples [33]. The steady state PL spectrum was recorded using a 405 nm diode laser (CNI Laser) excitation with the help of a PL spectrometer (Horiba Jobin Yvon, Fluoromax-4). Raman scattering measurement was carried out with a 514 nm Ar^+ laser excitation using a micro-Raman spectrometer (LabRAM HR-800, Jobin Yvon). The diffuse reflectivity of the samples was carried out using a commercial spectrophotometer (PerkinElmer, Lamda 950). Photocatalytic degradation of methylene blue (MB) (10^{-5} M aqueous solution) using Si NWs was performed in a commercial photochemical reactor (Lelesil Innovative Systems, Mumbai). A time programmable visible lamp was used for illuminating the sample with excitation wavelength 390–730 nm.

3. Results and discussions

3.1. Morphology and structure

Fig. 1(a) shows the FESEM top-view micrographs of Ag NPs on Si wafer (sample SiAg1). The diameter of the Ag NPs is distributed

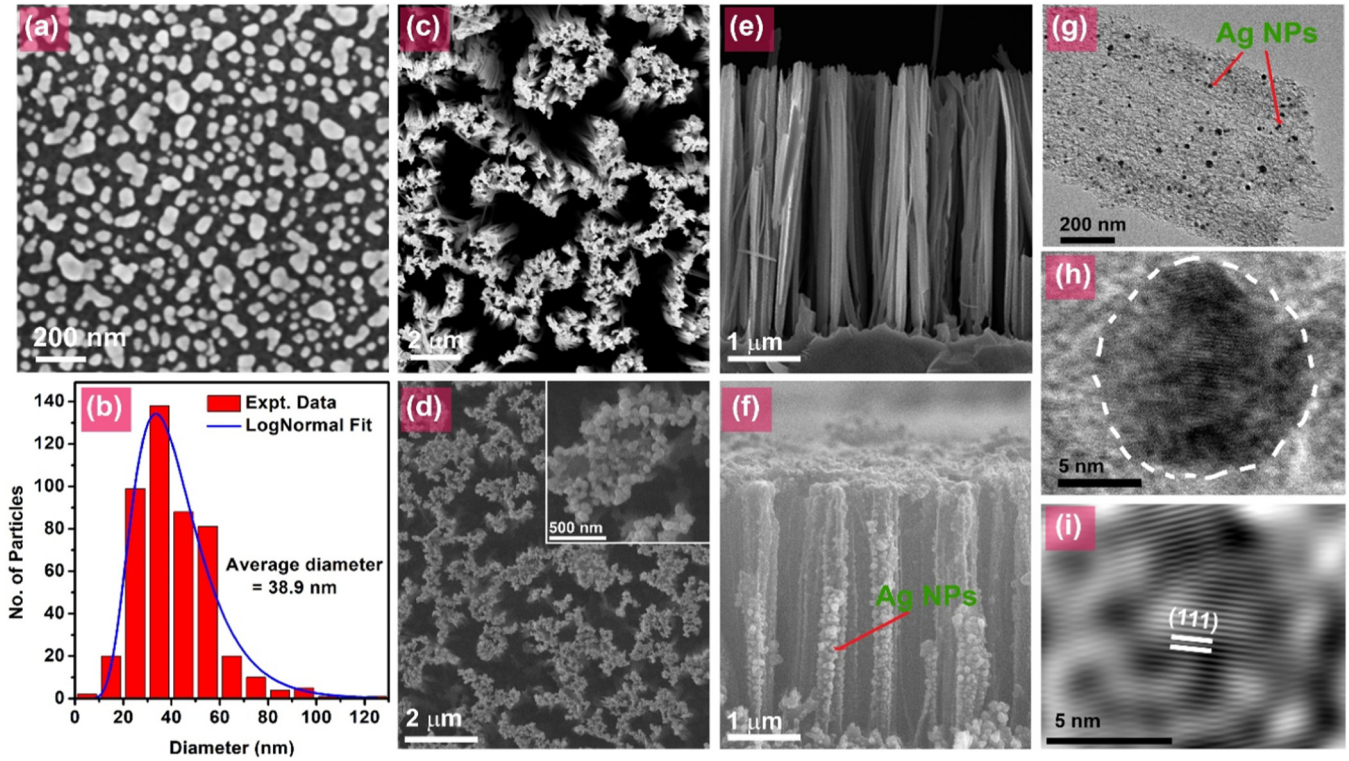

Fig. 1. (a) FESEM top-view micrographs of the sample SiAg1. (b) The diameter distribution of Ag NPs and its lognormal fitting. FESEM top-view micrographs of the samples: (c) NW and (d) NWAg1. The enlarged portion is shown as an inset of (d). (e, f) Corresponding cross-sectional images of the NWs. The presence of the Ag NPs is indicated with arrows. (g) TEM image of single Si NW decorated with the Ag NPs. (h) The HRTEM lattice image and of Ag NP on Si NW surface. The size of the Ag NP is estimated by the white dashed line. (i) corresponding IFFT image (magnified) confirms the (1 1 1) plane of Ag.

over a wide range (~10–100 nm), as shown in Fig. 1(b). The size distribution of the Ag NPs on Si wafer follows the typical lognormal distribution with an average diameter of 38.9 nm, as shown by the fitted curve. Fig. 1(c) and (d) shows the FESEM top-view micrographs of the Si NWs in sample NW and NWAg1, respectively, while (e, f) represent the corresponding cross-sectional view images. The enlarged top view of Ag@Si NWs is shown as an inset of Fig. 1(d). The FESEM images show the decoration of the Ag NPs on the top, sidewall and bottom of the Si NWs. It is found that the Ag NPs are agglomerated near the top of the NWs. Note that the Si NWs fabricated by MACE process tend to bend at the upper end and hence form bundles with tapered-like morphology [10]. During the post-growth decoration of Ag NPs, the top and upper side of the tapered bundles are covered with higher density of Ag NPs [34]. The Ag NPs on Si has a tendency to agglomerate and form Ag dendrites, when the sample is immersed for longer duration in $HF/AgNO_3$ [21,35]. In the present case, we have dipped the Si NWs in $HF/AgNO_3$ for a few seconds. Therefore, we obtained agglomerated/high density Ag NPs at the top of the Si NWs, while the density of Ag NPs on rest of the parts of the Si NWs is comparatively low. We believe that the ultrathin gaps between the Si NWs do not allow the $HF/AgNO_3$ solution to come to the bottom side of the NWs to decorate with Ag NPs. Note that the bigger size Ag NPs and their clusters are only visible from the FESEM images and thus the average NP diameter is quite large in Fig. 1(b). TEM analysis provides a detailed view of surface morphology of individual mesoporous Si NW decorated with the Ag NPs. Fig. 1(g) shows the TEM image of single Si NW decorated with the Ag NPs. Note that the Ag NP decoration process is statistically random for longer time of deposition. Fig. 1(h) and (i) show the HRTEM lattice images and corresponding IFFT images (magnified) of the Ag NP on Si NW surface. Fig. 1(i) confirms that the Ag NPs are single crystalline and (1 1 1) oriented.

In order to investigate the chemical composition, different oxidation states and defects, XPS studies were carried out on the Si NWs before and after Ag NPs decoration. Fig. 2 shows the comparison of the core level XPS spectra of the samples NW and NWAg1 for: (a) Si 2p, (b) Ag 3d and (c) O 1s peaks. It is clear from Fig. 2(a) that the ~99.4 eV peak corresponding to neutral Si is diminished after Ag NPs decoration, while the other broad peak centered at ~103.0 eV corresponding to different sub-oxides of Si is unaltered. XPS provides the surface property of the sample and information comes only from the first few nm layer. Note that the Ag NPs are agglomerated on the top of the Si NWs in case of sample NWAg1 and thus the neutral Si peak of the HS sample is diminished in Si 2p core level XPS spectrum. The Ag 3d core level XPS spectrum in Fig. 2(b) confirms the presence of Ag NPs in the HS sample. The Ag $3d_{5/2}$ and Ag $3d_{3/2}$ peaks are broad and indicate the presence of Ag_2O NPs, which is also consistent with the broad O 1s XPS core level spectrum of the HS sample in Fig. 2(c). In order to understand the contribution of metallic Ag and Ag_2O in the Ag 3d core level XPS spectrum, we have fitted each of the asymmetric bands corresponding to Ag $3d_{5/2}$ and Ag $3d_{3/2}$ by two gaussian peaks (Fig. S1, Supplementary Material). The Gaussian deconvolution shows that the system contains 12.2% of Ag^+ and 87.8% of metallic Ag. Thus, minor presence of Ag_2O is revealed from the XPS analysis.

Supplementary data associated with this article can be found, in the online version, at https://doi.org/10.1016/j.jcis.2018.07.123.

3.2. Optical properties of metal NP decorated Si NWs

3.2.1. Photoluminescence study

The MACE grown Si NWs (Sample NW) exhibit high intensity, broad visible-NIR PL [8–11]. Due to the mesoporous nature of the Si NWs, the Si NW surface is covered with arbitrary shaped

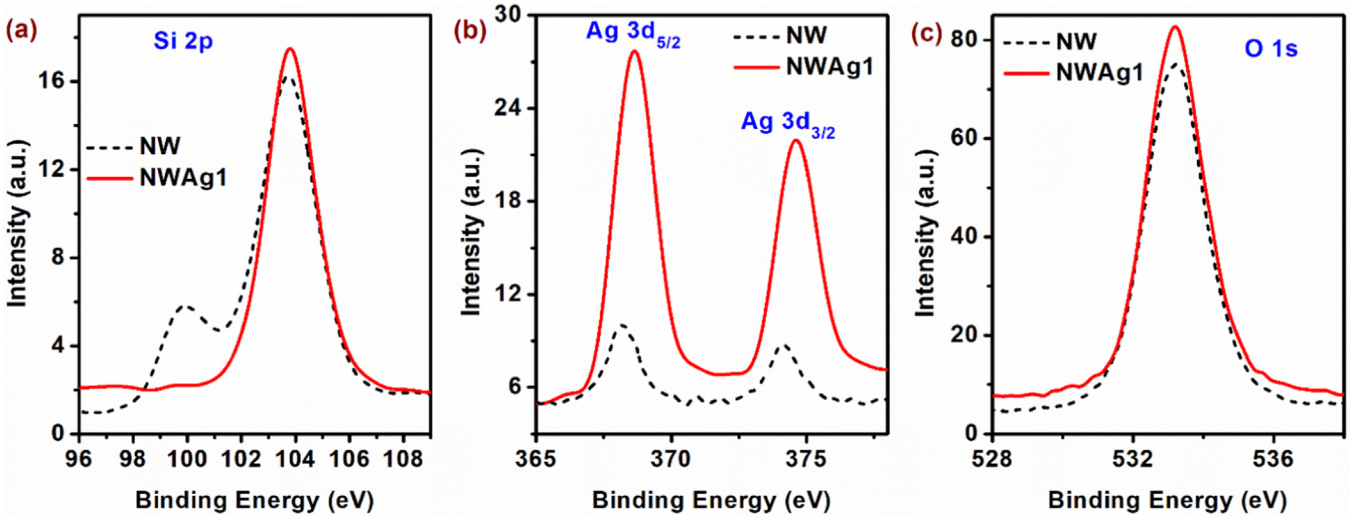

Fig. 2. Comparison of the core level XPS spectra of the sample NW and NWAg1: (a) Si 2p, (b) Ag 3d and (c) O 1s.

quantum size Si NCs [8–11,32]. Our XPS results also reveal that the Si NWs/NCs are covered with a native oxide layer, which is oxygen deficient, and thus, nonbridging oxygen hole center (NBOHC) defects are present in the SiO_x structure [8,9]. Based on the previous reports, it is believed that the broad visible PL emission from MACE grown Si NWs arises from the QC effect in Si NCs and NBOHC defects at the interface of Si—SiO_x [8–11]. In order to understand the effect of Ag NPs on the PL emission of the MACE grown Si NWs/NCs, we have measured the PL spectra of the bare Si NWs and Ag NPs decorated Si NWs under identical conditions. Fig. 3 (a) shows the comparison of the PL spectra of the sample NW and NWAg1, while 3(b) shows the comparison of PL spectra of Ag@Si NWs for different thickness of Ag NPs.

It is clear that after the Ag NP decoration, the PL intensity of the sample is reduced. Fig. 3(b) confirms that the PL intensity of Si NWs gradually decreases with the Ag NP loading and the sample NWAg4 has the lowest PL intensity among all samples. Sample NW2 shows the similar trend in PL spectra after Ag NP decoration, as shown in Fig. S2(a) (Supplementary Material). Note that Ag NPs were deposited by a chemical process, and during the deposition, Ag NPs may have filled the pore regions/sites of the Si NWs and light reaching the Si NWs/NCs is reduced. The decrease of PL intensity from Si NWs after Ag NP decoration depends up on several factors, such as: (a) surface covering by Ag NPs, which prevent the direct excitation of the mesoporous Si NWs, (b) reabsorption of the emitted light of Si NWs/NCs by the Ag NPs, (c) partial removal of the radiative sites (NBOHC defects) in the Si NWs etc. Fig. S2(b) (Supplementary Material) shows that the integrated PL intensity of the Si NWs decreases rapidly with Ag NP coating for 6–8 s. Note that the density of Ag NPs on the surface of Si NWs in $HF/AgNO_3$ solution does not follow a linear behavior with the deposition time. Earlier reports suggest that the rate of the Ag NP formation rate depends upon several condition, such as the $HF:AgNO_3$ relative concentration, resistivity of the Si NWs, reaction temperature etc. The PL spectra of the HS samples originate from the radiative sites in the mesoporous Si NWs and the Ag NPs (discussed later). The contribution of the later is very low as compared to the former (Si NWs). Hence, the PL intensities of the HS samples are extremely low, in which the Ag NPs are grown for longer duration in $HF/AgNO_3$.

In order to understand the effect of other noble metal NPs on the PL spectra of MACE grown Si NWs/NCs, we have recorded the PL spectra of Si NWs decorated with different metal and bimetal NPs, measured under identical conditions. Fig. S3 (Supplementary Material) shows the comparison of the PL spectra of the sample NW before and after Au NP and AuPd bimetal NP decoration. The decoration process for Au and AuPd bimetal on Si NWs are provided in the Supplementary Material (Section 1). After metal NP decoration, the PL intensity of the sample is reduced in each case. Previous reports have shown the enhancement of PL intensity instead of decrease, due to SPR effect of the NPs. For example, in case of Si NCs in a SiO_2 matrix, the highest reported PL intensity enhancement in presence of nanoscale Ag island arrays is 7-fold [36], while it is only 4-fold in case of Si NWs [37]. Recently, 8-fold enhanced PL was reported for porous Si NWs after Au NPs decoration [38]. Similar enhancement by a factor of 3 in PL intensity in Si NWs/Au NPs composite was reported by Au-catalyzed chemical etching method [27]. The enhancement in PL efficiency was explained in terms of radiative energy exchange between Si NCs and metal NPs due to enhanced radiative coupling of exciton-plasmon [27,39]. In the present case, we observed partial quenching of PL intensity for all cases. The reduced intensity of PL can be explained by the Schottky junction effect between the Si and the metal NPs. Because of the differences in the Fermi levels (EF) between the metal and the Si, a Schottky barrier is introduced between the metal NPs and Si NWs/NCs. The built-in potential at the Schottky junction can facilitate the efficient separation of photogenerated e-h pairs and reduce the radiative recombination, which results in the decreased PL intensity. Shao et al. reported that the high work function (Φ) of the noble metals accelerates the electron from conduction band (CB) of semiconductor to metal and reduce the radiative recombination rate [16]. Interestingly, this process is helpful for the photocatalytic degradation of the organic dye (discussed later) [8,9]. Furthermore, the electronegativity of the noble metal (Au, Ag or AuPd bimetal) is higher than that of Si [8]. Hence, these metal NPs can accelerate the separation of photoinduced e-h pairs better, which can decrease the radiative recombination, hence the reduced PL intensity.

It is clear from Fig. 3(a,b) that the PL spectrum of the sample NW becomes much broader after Ag NPs decoration and it covers the visible-NIR range (1.4–3 eV). In order to understand the contribution of Ag NPs in the broad PL emission, we have measured the PL spectrum of the sample SiAg1 and the results are shown in Fig. 3(c). The PL spectrum of NWAg1 was fitted by 3 Gaussian bands to understand the effect of different species on the broad visible PL. Fig. 3(d) shows the deconvoluted PL spectrum of the sample NWAg1 (deposition time 2 sec). Interestingly, the peak centered at ~2.4 eV (Peak 3) is also present in case of Ag NPs on bulk Si

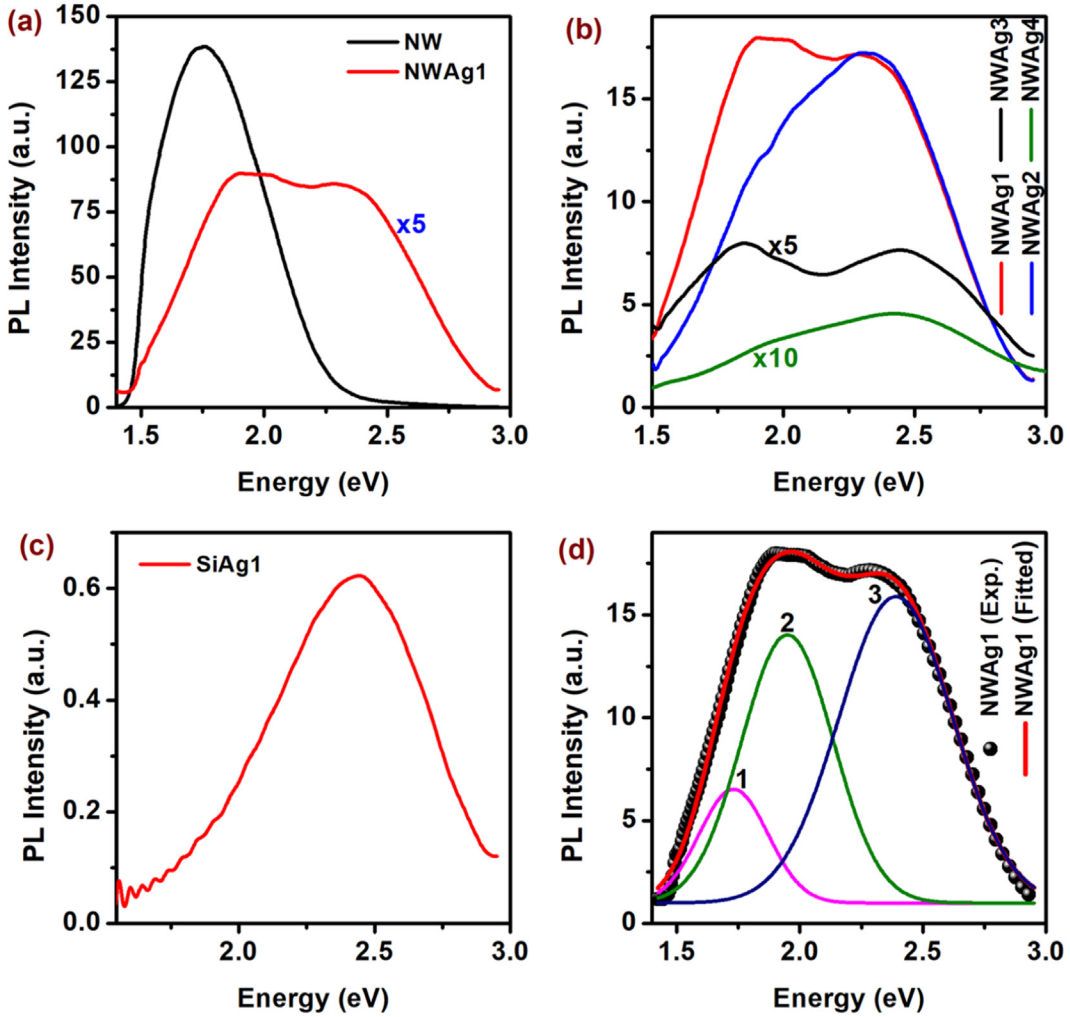

Fig. 3. Comparison of the PL spectra of samples NW and NWAg1. The PL spectrum of the sample NWAg1 is scaled up by a factor 5 to enable comparison. (c) Comparison of the PL spectra of the sample NWAg1, NWAg2, NWAg3 and NWAg4. PL spectra of the sample NWAg3 and NWAg4 are scaled up by a factor 5 and 10, respectively, to enable comparison. (d) PL spectrum of the sample SiAg1. (d) The fitted PL spectrum of the sample NWAg1. In each case, PL measurement was carried out with 405 nm laser excitation at 10 mW power (at source).

wafer (Fig. 3(c)). This peak is generally attributed to electronic transitions between the upper 'd' band and conduction 'sp' band of Ag NPs [40]. Yeshchenko et al. reported that this PL of Ag NPs is due to the radiative decay of SPR excited in NPs [41]. It is clear from the XPS spectra that the mixed states of Ag and Ag_2O are present in the sample NWAg1. According to Gangopadhyay et al., the 2.4 eV PL is attributed to the band-to-band radiative transition in Ag_2O [42]. Other two peaks, i.e. peak 1 and peak 2 in Fig. 3(d), centered at ~1.73 eV and ~1.94 eV are due to the QC effect in Si NCs and NBOHC defects in the interface of Si—SiO_x, respectively [8–11]. It is interesting to note that the broad visible PL from the Ag@Si NWs covers the entire visible range, which is significant for white light emitting applications.

In order to understand the white light content in the PL spectra, the Commission International de l'Eclairage (CIE) coordinates were calculated for the PL spectra of the samples. The CIE coordinates were calculated to be (0.6059, 0.3823), (0.3994, 0.4335), (0.3737, 0.4412) and (0.3543, 0.3785) for the samples NW, NWAg1, NWAg2 and NWAg3, respectively. The emission characteristics of the Ag@Si NWs are illustrated in the CIE 1931 chromaticity diagram shown in Fig. 4. It is very clear that the CIE coordinate for the sample NW is in the red region and after Ag NPs decoration, the CIE coordinates lie very close to that of the pure white light (0.33, 0.33) [43]. Though the intensity of the PL of Si NWs/NCs is reduced

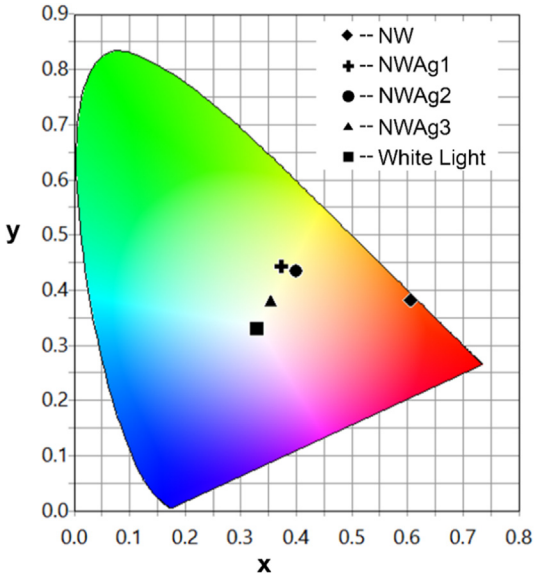

Fig. 4. Chromaticity diagram showing the CIE coordinates of the samples NW, NWAg1, NWAg2, NWAg3 and pure white light.

after Ag NPs decoration, the white light emission opens up the possibility of using Ag@Si NWs in the fabrication of white light LED.

4. Photocatalysis

The excitons generated within the mesoporous Si NWs could be energetic enough to drive photoelectrochemical reactions due to its wide range of optical absorption with high intensity and broad visible emission centered near the red-infrared region. It was reported that the electron deficient Si—H surface states present in the MACE grown Si NWs/NCs samples serve as electron sink and hence accelerate the separation of photoinduced e-h pairs, which facilitate the photocatalytic activity of the Si NWs/NCs [8,9]. We have obtained the enhanced photocatalytic activity of Si NWs after Ag NPs decoration. Fig. 5(a) shows the photodegradation efficiencies of the sample NW, NWAg1, SiAg1 and bulk Si. MB is used as the target dye molecule for the photodegradation experiment. We have also studied the visible light photocatalytic activities of different metal NP decorated Si NWs/NCs for the degradation of MB. Fig. 5(b) shows the comparison of the photodegradation efficiencies of sample NW decorated with different metal NPs, while Fig. 5(c) shows the corresponding rate constant (k) of the respective samples considering the 1st order rate kinetics [8,9]. The calculation of k is shown in the Supplementary Material (Section 2). We observed that after the metal NPs decoration, photodegradation efficiency increases for some of the samples (NWAg1 and NWAuPd), while it decreases for the sample NWAu. This type of mixed photocatalytic behavior was also observed in earlier studies [15,16]. For example, Shao et al. have shown that the photodegradation efficiency (in RhB) of H—Si NWs is higher than the Ag, Au or Pd coated Si NWs [16]. The charge separation capabilities of Si—H bonds are better for some of the noble metals. In the present case, the metal deposition partially removes/covers Si—H bonds in the samples, which are responsible for the decrease in the photocatalytic efficiency of NWAu.

Note that we have observed the enhanced photocatalytic degradation performance for the samples NWAg1 and NWAuPd. The enhancement can be explained in the following way. The differences in the Fermi levels can introduce a Schottky barrier between the metal NPs and Si NWs/NCs. The schematic diagram of the MACE grown mesoporous Si NW arrays decorated with metal NPs along with the band alignment is shown in Fig. 6. The possible charge separation in presence of Si—H bonds and metal NPs, and the dye degradation mechanism are schematically illustrated in Fig. 6. The built-in potential at the Schottky junction can facilitate the efficient separation of photogenerated e-h pairs and influence the degradation of the dye strongly [8,9]. The charge separation occurs due to the charge transfer from the CB of Si to the metal. Also, the additional effect of charge separation (instead of only Si—H) in sample NWAg1 and NWAuPd is responsible for the enhanced rate constant as shown in Fig. 5(c). On the other hand, the electronegativity of the noble metals Au, Ag or AuPd bimetal is higher than that of Si [8]. Hence, these metal NPs can accelerate the separation of photoinduced e-h pairs better, which can increase the photocatalytic activity of the HS samples [8,9,15,16]. Shao et al. reported that the photocatalytic activity of metal-semiconductor catalysts depends largely on the electron work function of metals, which is a key parameter in the electron transfer process from conduction band of semiconductor to metal [16]. The charge transfer process is enhanced for the metal with higher Φ [16]. Pd has a higher value of Φ (5.12 eV) as compared to the other metals we have used in the present study. Thus, the rate

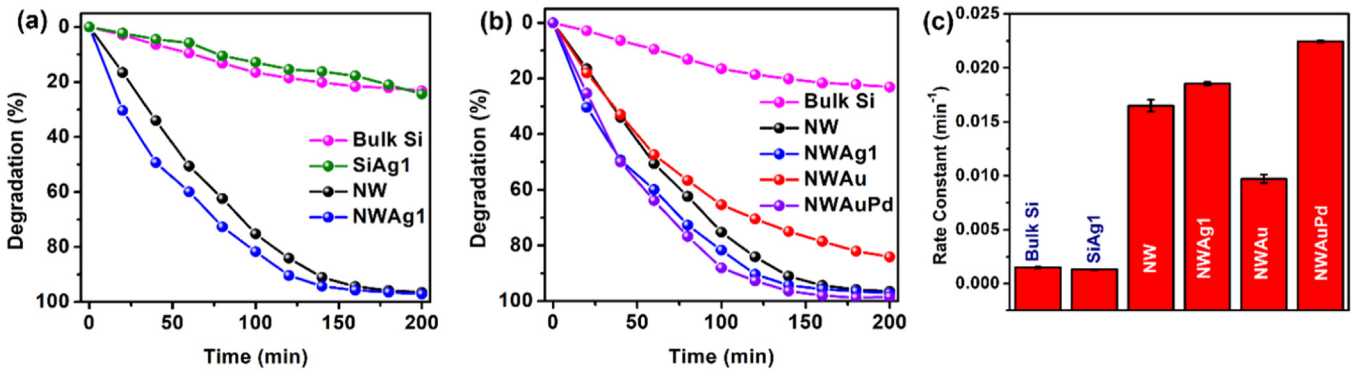

Fig. 5. (a) Comparison of the photocatalytic degradation efficiencies of sample NW, NWAg1, SiAg1 and bulk Si. (b) Comparison of the photodegradation efficiencies of sample NW and its heterostructure with different metal NPs. (c) Corresponding degradation rate constants for different samples.

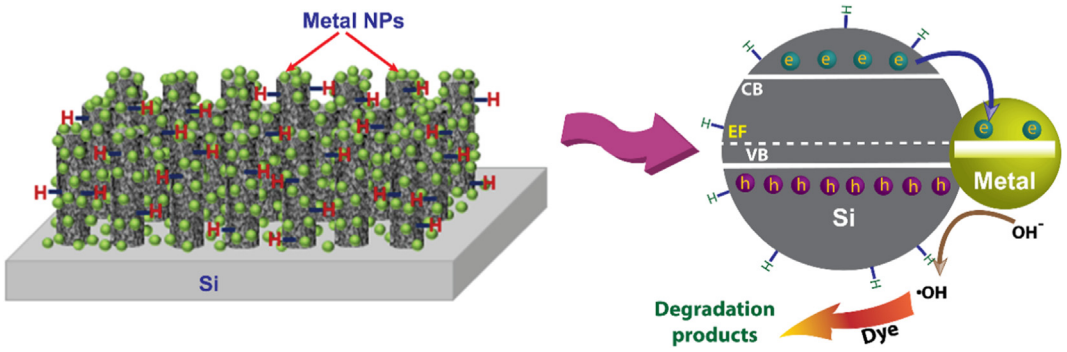

Fig. 6. Illustration of photocatalysis mechanism by metal NPs decorated on h-terminated mesoporous Si NWs showing the e-h pair production, effective charge separation and subsequent dye degradation.

constant is maximum when Pd is incorporated as bimetal in AuPd coated Si NWs/NCs. Liao et al. reported that AuPd bimetal decoration on Si NWs results in the higher degradation rate of p-nitroaniline as compared to the single metal decorated Si NWs [22]. However, SPR related broad visible absorption due to these metal NPs can also function as the catalysts to facilitate certain redox reactions to degrade MB dye [8,9,44]. Thus, after Ag decoration, the PL intensity decreases (Fig. 3(a)), which confirm the effective charge separation in the sample NWAg1 and hence the enhanced photodegradation efficiency. However, the enhancement of is not very significant due to the partial removal of Si—H bonds from the Si NW surface during the Ag NP decoration. Thus, due to the competing effect, resultant rate constant of NWAg1 is marginally improved after intentional Ag decoration. Note that the partial contribution of Ag_2O in the photocatalytic efficiency enhancement cannot be ruled out, as the same has been detected in the XPS analysis. In this case, charge separation at the heterojunction of Si/Ag_2O may contribute to the enhanced photocatalytic degradation of organic dyes.

5. Optical sensing and SERS detection using mesoporous Si NWs

Metal NPs decorated Si NWs provide excellent charge transport properties, biocompatibility and environment-friendly nature and are demonstrated as excellent candidate for sensing of chemical and biological molecules [23,24,26,28,45–48]. Different sensitive methods, including optical-based detection (surface enhanced Raman scattering (SERS) or fluorescence), mechanical based detection (cantilevers), and electrical-based detection (FET) are attractive in a number of sensing applications [23,24,26,28,45–48]. Among these methods, optical-based detection process is most versatile and non-destructive method for the selective, sensitive and quantitative detection of bio-chemical species. Here, we have studied the optical sensors based on Ag@Si NWs.

5.1. Fluorescence based detection

Optical sensor based on PL spectroscopy is one of the well-known sensing techniques for the detection of biological species [19,24,30,49,50]. Metal NPs decorated Si NWs have been used as a fluorescence sensor for the selective detection of bio-chemical species, gas molecules and heavy metal ions [24,30,49]. We have used Ag@Si NWs for the detection of the organic molecule RhB and MB by the PL based sensing technique. The change in PL spectra of the sample NWAg1 was examined in presence of the organic molecule at different concentrations. For doing so, we have kept the pieces of sample NWAg1 in an aqueous solution of organic

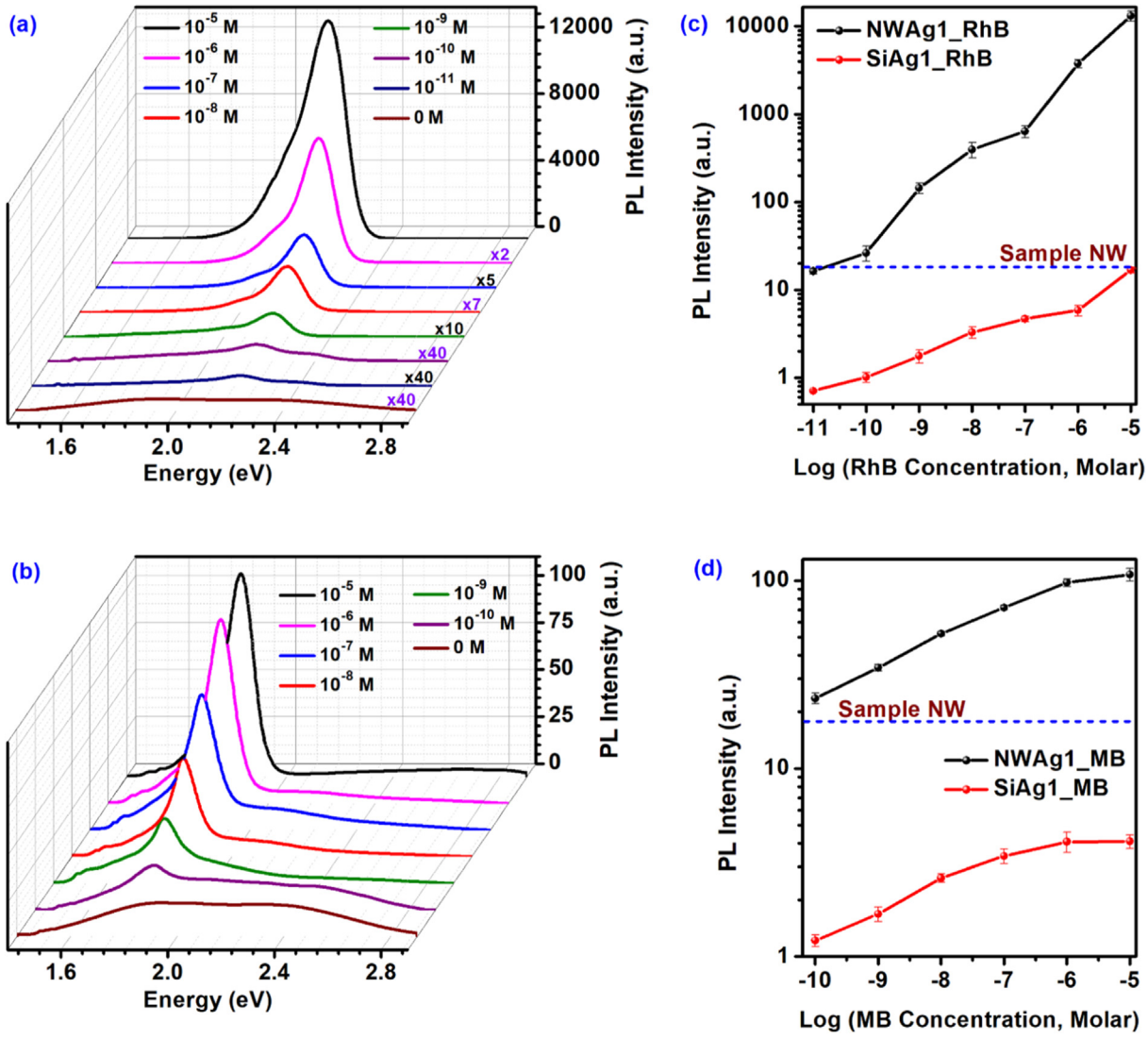

Fig. 7. (a, b) Comparison of the PL spectra of NWAg1 for different concentrations of RhB and MB, respectively. (c, d) PL peak intensity of NWAg1 as a function of RhB and MB concentration, respectively. The PL intensity of sample SiAg1 is also shown for comparison.

molecules with different concentrations. We performed a similar experiment in case of sample SiAg1 also. In each case, the samples are kept in dark for 12 h for better adsorption of the organic molecules. Fig. 7(a, b) show a comparison of the PL spectra of the sample NWAg1 in presence of RhB and MB at different concentrations, respectively. Fig. 7(c, d) show the change in PL peak intensity of sample NWAg1 as a function of RhB and MB concentration, respectively. The variation of PL intensity of sample SiAg1 with the respective organic molecule concentration is also compared in Fig. 7(c, d). The sample NWAg1 can detect 10^{-11} M concentration of RhB and10^{-10} M concentration of MB very efficiently. We have observed that in each case of Fig. 7(a) and (b), PL intensity of the organic dyes (RhB and MB) on NWAg1 is enhanced with increasing the concentration of organic molecule. The rate of increase in PL intensity is higher for RhB (Fig. 7(c)) than MB (Fig. 7(d)) due to high PL quantum yield (QY) of RhB. Note that the PL intensity of NWAg1 is much higher than that of SiAg1 in each concentration of RhB or MB. We have calculated the enhancement factor of PL intensity of sample NWAg1 over sample SiAg1 in each concentration of RhB and MB (Fig. S4, Supplementary Material). It is clear that the enhancement factor gradually increases with the concentration of the organic molecule. This suggests that the sensitivity decreases with lowering of the target molecule concentration. However, we obtained enhanced PL emission of RhB/MB on the surface of Ag@Si NWs as compared to that of on Ag NPs on bulk Si (sample SiAg1). The possible reasons for this enhancement are: (a) enormous surface area of the mesoporous Si NWs, and (b) surface plasmon resonance (SPR) induced absorption due to the presence of the Ag NPs.

The MACE grown Si NWs have a mesoporous surface, which leads to the enormous surface area. Due to this, large number of organic molecules is exposed to laser excitation and emits high intensity PL. On the other hand, the porous sites act as the platform to hold the RhB/MB molecule to its surface. Due to this, the PL intensity of RhB/MB is much higher in sample NWAg1 as compared to the SiAg1. However, only surface area can not account for the enormous enhancement of PL intensity of RhB/MB (22.9 times enhancement of RhB in 10^{-11} M concentration and 19.4 times enhancement of MB in 10^{-10} M concentration).

We observed that the Ag@Si NWs have very high absorbance (Fig. S5, Supplementary Material) due to the SPR absorption effect in Ag NPs. This SPR effect is one of the main reason of enhanced PL intensity of RhB/MB on Ag@Si NWs. Note that this SPR effect is also applicable for sample SiAg1 and thus, we obtained considerable PL response of Ag NPs on bulk Si wafer. The combined effect of high surface area of Si NWs and SPR in Ag NPs lead to the high range of detection in case of Ag@Si NWs. So, the Ag NPs decorated Si NWs can be used as fluorescence-based sensor for the selective detection of organic species. Note that the detection range of the sensor can be increased by tuning some crucial parameters, such as: (a) length of the Si NWs, (b) porosity of the Si NWs, (c) size, density and thickness of the Ag NPs, (e) the optical excitation intensity, and (f) detector sensitivity of the spectrometer.

5.2. SERS detection

Optical based SERS detection by metal NPs decorated Si NW HSs is another efficient way of sensing chemical and biological molecules with surface-seeking groups, since only molecules on or near the metal surface experience the large near-field enhancements upon resonant plasmon excitation. Si NWs coated with metal NPs, mainly Ag, Au, Pd, Cu, and Pt have been used as SERS effective substrates for sensing a variety of inorganic and organic molecules [21,51–53]. In order to understand the SERS effect in Ag@Si NWs, we have chosen MB and Rose Bengal (RB) as the target molecules. We have carried out Raman measurement of MB and RB with different low concentrations (down to10^{-12} M for MB and 10^{-11} M for RB) on the sample NWAg1. The samples were kept in MB/RB solution with different concentration in dark for 12 h to enable high adsorption. Raman measurement of the samples was carried out with 514 nm laser excitation with 1.2 mW laser power. Fig. 8(a, b) shows the SERS spectra of MB and RB, respectively, for the sample NWAg1. From Fig. 8(a), we have obtained high intensity peaks centered at ~1580 cm^{-1} and ~1348 cm^{-1} at each concentration of MB. The ~1580 cm^{-1} peak is attributed to aromatic ring vibrations, while ~1348 cm^{-1} peak is due to C—N symmetrical and asymmetrical vibration in MB structure [51]. In case of RB in Fig. 8(b), we have observed high intensity peaks at ~1375 cm^{-1} and ~1590 cm^{-1}, which is due to C—C stretching and C=C symmetric stretching in ring [25]. These high intensity peaks are prominent enough to detect MB and RB, even at extremely low concentration, i.e. 10^{-12} M for MB and 10^{-11} M for RB, respectively. We did not observe any peak corresponding to MB or RB in case of sample SiAg1, when the concentration is $<10^{-6}$ M. We have compared the Raman spectra of the sample NWAg1 and SiAg1 in Fig. S6(a, b) (Supplementary Material) for fixed concentration (10^{-4} M) of MB and RB, respectively. It is observed from Fig. S6(a) (Supplementary Material) that the peaks at ~1580 cm^{-1} and ~1348 cm^{-1} of sample NWAg1 are enhanced by ~3.5 times and ~4.1 times, respectively, as compared to that of SiAg1.

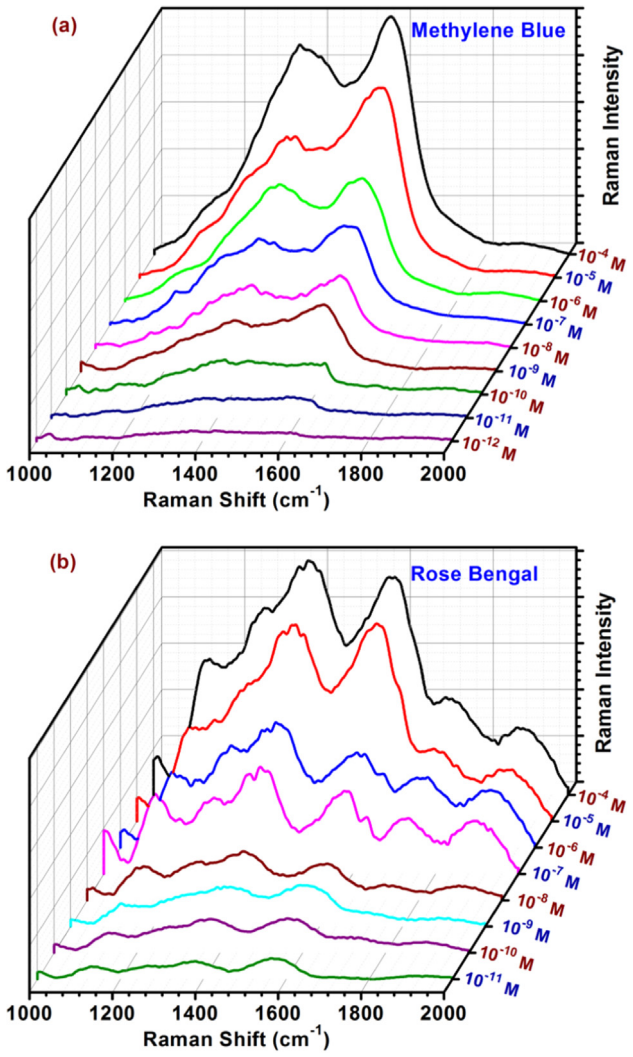

Fig. 8. SERS sensing behavior of the sample NWAg1 for different concentrations of: (a) MB and (b) RB.

Similarly, in Fig. S6(a) (Supplementary Material), we observed that the peaks at ~1590 cm^{-1} and ~1375 cm^{-1} of sample NWAg1 are enhanced by ~5.3 times and ~6.7 times, respectively, as compared to the SiAg1. This is due to the SERS effect of Ag NPs on the Si NWs. These results are very promising for the high sensitive SERS detection of organic and bio-molecules by Ag@Si NWs.

In order to understand the SERS efficiency of the sample NWAg1, we have calculated the enhancement factor (EF) according to the following equation: [51–53]

where I_R and I_{SERS} are the Raman intensity of the target molecule on bulk Si and SERS substrates for the same band (~1580 cm^{-1} for MB and ~1375 cm^{-1} for RB, which are the most prominent peaks for these target molecules), C_{SERS} and C_R are the concentration measured from the SERS sample and the reference sample (the target molecule in absence of SERS substrate). Table 2 shows the SERS efficiency of sample NWAg1 with measurement parameters for the target molecules MB and RB. Earlier reports suggest that EF of Ag@Si NWs is 10^8–10^{10} for the detection of Sudan dyes and DNA [52,53]. No details about EF of Ag@Si NWs are present in the literature for the detection of MB and RB. Here, we have observed significantly high values of EF as ~10^8 and ~10^9 for the detection of MB and RB, respectively, which are similar to the reported values on other systems.

Next, we have studied the recycling ability of the present sensor by investigating the sensing experiment repeatedly for constant MB concentration i.e. 10^{-6} M. After each cycle, the sample NWAg1 was cleaned by using 0.5 M sodium borohydride ($NaBH_4$), which is a well-known reductant for the fast and complete removal of the trace MB [51]. After MB cleaning, the sample is rinsed several times with DI water before another SERS measurement. Fig. 9 shows the Raman spectra of MB for different cycles. The Raman spectra of the sample after MB removal are also plotted together. It is observed that most intense Raman peak of MB is reduced to ~50% after 10th cycle. Thus, Ag@Si NWs can be used for multiple cycles for the detection of organic molecules. The decrease in the Raman signal of MB after several cycles suggests that the Si NWs as well as Ag NPs are partially oxidized by the adsorbed MB, which leads to the decrease in SERS sensitivity.

Table 2
SERS efficiency of sample NWAg1 with measurement parameters for the target molecules MB and RB.

Target	C_{SERS} (M)	I_{SERS}	C_R (M)	I_R	EF
MB	10^{-11}	250	10^{-4}	12	2.9×10^8
RB	10^{-11}	625	10^{-4}	2.5	2.5×10^9

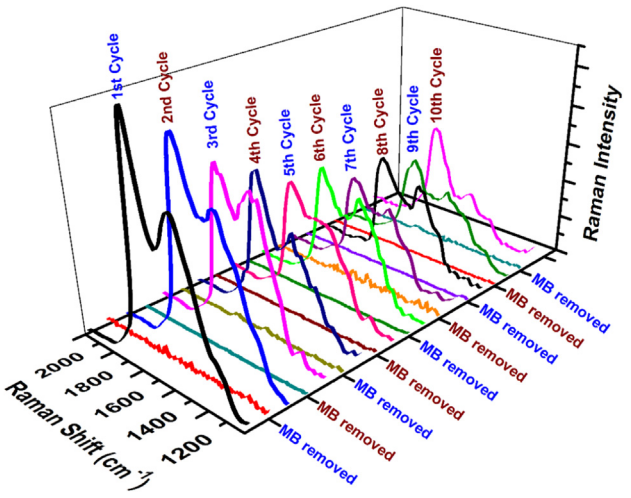

Fig. 9. Cyclic stability of SERS sensing behavior of NWAg1 as substrate, keeping the concentration of MB fixed for different cycles.

Our results open up the possibility of using Ag@Si NW HSs in white light display application as well as organic waste treatment and hydrogen production by photocatalytic water splitting. These HSs are preferable for sensitive and selective label-free detection of different bio-chemical species using nondestructive optical spectroscopy techniques. Therefore, Ag@Si NWs system has great potential in the multi-directional nanotechnology applications.

6. Conclusion

Our study reveals the superior optoelectronic and photophysical properties of Ag NP decorated mesoporous Si NW arrays. We have fabricated Ag NP decorated mesoporous Si NWs by a simple and cost-effective chemical process. The Ag@Si NWs show broad-band white light emission, efficient photocatalysis and excellent sensitivity for the detection of organic molecules over a wide range of concentrations. The broad-band white light emission from the Ag@Si NWs was explained on the basis of emission from Ag NPs, QC effect in Si NCs and the NBOHC defects in the Si—SiO_x interface. High work function of the noble metal NPs facilitates the effective separation of the photoinduced electron-hole pairs in Si NWs, which enables the Ag@Si NWs to exhibit high photocatalytic efficiency. The Ag@Si NWs exhibited high potential and sensitivity for the selective and quantitative detection of different organic molecules, with an extremely low concentration down to 10^{-12} M by SERS effective Raman analysis and 10^{-11} M by fluorescence detection. Plenty of prospects are left to the researchers to improve the multi-functional photophysical properties of Ag@Si NW arrays. These versatile properties of the Ag@Si NWs open up huge opportunities for a variety of energy and environmental applications, such as white LED, solar cell, artificial photosynthesis, disposal of organic pollutant and bio-chemical sensors.

Acknowledgements

We acknowledge the financial support from CSIR (Grant No. 03 (1270)/13/EMR-II) and MEITY (Grant No. 5(9)/2012-NANO(VOL-II)) for carrying out part of this work. Central Instruments Facility, IIT Guwahati is acknowledged for the TEM and Raman facilities. We also acknowledge Centre for Excellence in Nanoelectronics & Theranostic Devices, IIT Guwahati for conducting our research. We also thank Prof. Fujii, Kobe University, for his help in the XPS measurement. We acknowledge Brain Korea 21 Program and Prof. Gyu-Chul Yi, Seoul National University for carrying out part of this work.

References

[1] M. Otto, M. Algasinger, H. Branz, B. Gesemann, T. Gimpel, K. Füchsel, T. Käsebier, S. Kontermann, S. Koynov, X. Li, V. Naumann, J. Oh, A.N. Sprafke, J. Ziegler, M. Zilk, R.B. Wehrspohn, Black Silicon Photovoltaics, Adv. Optical Mater. 3 (2) (2015) 147.
[2] V. Schmidt, J.V. Wittemann, U. Gösele, Growth, thermodynamics, and electrical properties of silicon nanowires, Chem. Rev. 110 (1) (2010) 361.
[3] K.-Q. Peng, S.-T. Lee, Silicon nanowires for photovoltaic solar energy conversion, Adv. Mater. 23 (2) (2011) 198.
[4] M. Shao, D.D.D. Ma, S.-T. Lee, Silicon nanowires – synthesis, properties, and applications, Eur. J. Inorg. Chem. 2010 (27) (2010) 4264.
[5] K.-Q. Peng, X. Wang, L. Li, Y. Hu, S.-T. Lee, Silicon nanowires for advanced energy conversion and storage, Nano Today 8 (1) (2013) 75.
[6] X. Liu, P.R. Coxon, M. Peters, B. Hoex, J.M. Cole, D.J. Fray, Black silicon: fabrication methods, properties and solar energy applications, Energy Environ. Sci. 7 (10) (2014) 3223.
[7] V. Schmidt, J.V. Wittemann, S. Senz, U. Gösele, Silicon nanowires: a review on aspects of their growth and their electrical properties, Adv. Mater. 21 (25–26) (2009) 2681.
[8] R. Ghosh, K. Imakita, M. Fujii, P.K. Giri, Effect of Ag/Au bilayer assisted etching on the strongly enhanced photoluminescence and visible light photocatalysis by Si nanowire arrays, Phys. Chem. Chem. Phys. 18 (2016) 7715.

[9] R. Ghosh, P.K. Giri, Efficient visible light photocatalysis and tunable photoluminescence from orientation controlled mesoporous si nanowires, RSC Adv. 6 (2016) 35365.
[10] R. Ghosh, P.K. Giri, K. Imakita, M. Fujii, Origin of visible and near-infrared photoluminescence from chemically etched Si nanowires decorated with arbitrarily shaped Si nanocrystals, Nanotechnology 25 (4) (2014) 045703.
[11] R. Ghosh, A. Pal, P.K. Giri, Quantitative analysis of the phonon confinement effect in arbitrarily shaped Si nanocrystals decorated on Si nanowires and its correlation with the photoluminescence spectrum, J. Raman Spec. 46 (7) (2015) 624.
[12] A. Convertino, M. Cuscunà, F. Martelli, M.G. Manera, R. Rella, Silica Nanowires decorated with metal nanoparticles for refractive index sensors: three-dimensional metal arrays and light trapping at plasmonic resonances, J. Phys. Chem. C 118 (1) (2014) 685.
[13] X. Wang, K.-Q. Peng, X.-J. Pan, X. Chen, Y. Yang, L. Li, X.-M. Meng, W.-J. Zhang, S.-T. Lee, High-performance silicon nanowire array photoelectrochemical solar cells through surface passivation and modification, Angew. Chem. Int. Ed. 50 (42) (2011) 9861.
[14] S.G. Yenchalwar, V.K. Azhagan, M.V. Shelke, Enhanced photoluminescence and photoactivity of plasmon sensitized nSiNWs/TiO_2 heterostructures, Phys. Chem. Chem. Phys. 16 (33) (2014) 17786.
[15] N. Megouda, Y. Cofininier, S. Szunerits, T. Hadjersi, O. ElKechai, R. Boukherroub, Photocatalytic activity of silicon nanowires under UV and visible light irradiation, Chem. Comm. 47 (3) (2011) 991.
[16] M. Shao, L. Cheng, X. Zhang, D.D.D. Ma, S.T. Lee, Excellent photocatalysis of HF-treated silicon nanowires, J. Am. Chem. Soc. 131 (49) (2009) 17738.
[17] N. Brahiti, T. Hadjersi, H. Menari, S. Amirouche, O. El Kechai, Enhanced photocatalytic degradation of methylene blue by metal-modified silicon nanowires, Mater. Res. Bul. 62 (2015) 30.
[18] C. Fang, A. Agarwal, E. Widjaja, M.V. Garland, S.M. Wong, L. Linn, N.M. Khalid, S. M. Salim, N. Balasubramanian, Metallization of silicon nanowires and sers response from a single metallized nanowire, Chem. Mater. 21 (15) (2009) 3542.
[19] R. Ghosh, R. Das, P.K. Giri, Label-free glucose detection over a wide dynamic range by mesoporous Si nanowires based on anomalous photoluminescence enhancement, Sens. Actuat. B: Chem. 260 (2018) 693.
[20] J. Ghosh, R. Ghosh, P.K. Giri, Mesoporous Si nanowire templated controlled fabrication of organometal halide perovskite nanoparticles with high photoluminescence quantum yield for light-emitting applications, ACS Appl. Nano Mater. 1 (2018) 1551.
[21] R. Ghosh, P.K. Giri, Silicon nanowire heterostructures for advanced energy and environmental applications: a review, Nanotechnology 28 (1) (2017) 012001.
[22] F. Liao, T. Wang, M. Shao, Silicon nanowires: applications in catalysis with distinctive surface property, J. Mater. Sci: Mater. Electron. 26 (7) (2015) 4722.
[23] M. Wipf, R.L. Stoop, A. Tarasov, K. Bedner, W. Fu, I.A. Wright, C.J. Martin, E.C. Constable, M. Calame, C. Schönenberger, Selective sodium sensing with gold-coated silicon nanowire field-effect transistors in a differential setup, ACS Nano 7 (7) (2013) 5978.
[24] S. Su, X. Wei, Y. Zhong, Y. Guo, Y. Su, Q. Huang, S.-T. Lee, C. Fan, Y. He, Silicon nanowire-based molecular beacons for high-sensitivity and sequence-specific DNA multiplexed analysis, ACS Nano 6 (3) (2012) 2582.
[25] A.M. Gabudean, M. Focsan, S. Astilean, Gold nanorods performing as dual-modal nanoprobes via metal-enhanced fluorescence (MEF) and surface-enhanced raman scattering (SERS), J. Phys. Chem. C 116 (22) (2012) 12240.
[26] T.-T. Xu, J.-A. Huang, L.-F. He, Y. He, S. Su, S.-T. Lee, Ordered silicon nanocones arrays for label-free DNA quantitative analysis by surface-enhanced Raman spectroscopy, Appl. Phys. Lett. 99 (15) (2011) 153116.
[27] M. Bassu, M.L. Strambini, G. Barillaro, F. Fuso, Light emission from silicon/gold nanoparticle systems, Appl. Phys. Lett. 97 (14) (2010) 143113.
[28] M.-W. Shao, M.-L. Zhang, N.-B. Wong, D.D.-d. Ma, H. Wang, W. Chen, S.-T. Lee, Ag-modified silicon nanowires substrate for ultrasensitive surface-enhanced Raman spectroscopy, Appl. Phys. Lett. 93 (23) (2008) 233118.
[29] K.K. Paul, R. Ghosh, P.K. Giri, Mechanism of strong visible light photocatalysis by Ag_2O-nanoparticle-decorated monoclinic TiO_2 (B) porous nanorods, Nanotechnology 27 (31) (2016) 315703.
[30] S. Zhuo, M. Shao, L. Cheng, R. Que, S. Zhuo, D.D. Duo Ma, S.-T. Lee, Surface-enhanced fluorescence of praseodymium ions (Pr^{3+}) on silver/silicon nanostructure, Appl. Phys. Lett. 96 (10) (2010) 103108.
[31] A. Pal, R. Ghosh, P.K. Giri, Early stages of growth of Si nanowires by metal assisted chemical etching: a scaling study, Appl. Phys. Lett. 107 (7) (2015) 072104.
[32] R. Ghosh, P.K. Giri, K. Imakita, M. Fujii, Photoluminescence signature of resonant energy transfer in ZnO coated Si nanocrystals decorated on vertical Si nanowires array, J. Alloy Compd. 638 (2015) 419.
[33] E.G. Barbagiovanni, L.V. Goncharova, P.J. Simpson, Electronic structure study of ion-implanted Si quantum dots in a SiO_2 matrix: analysis of quantum confinement theories, Phys. Rev. B 83 (3) (2011) 035112.
[34] V.S. Vendamani, S.V.S. Nageswara Rao, S. Venugopal Rao, D. Kanjilal, A.P. Pathak, Three-dimensional hybrid silicon nanostructures for surface enhanced Raman spectroscopy based molecular detection, J. Appl Phys. 123 (1) (2018) 014301.
[35] Z. Huang, N. Geyer, P. Werner, J. de Boor, U. Gosele, Metal-assisted chemical etching of silicon: a review, Adv. Mater. 23 (2011) 285.
[36] J.S. Biteen, N.S. Lewis, H.A. Atwater, H. Mertens, A. Polman, Spectral tuning of plasmon-enhanced silicon quantum dot luminescence, Appl. Phys. Lett. 88 (13) (2006) 131109.
[37] W. Chern, K. Hsu, I.S. Chun, B.P.D. Azeredo, N. Ahmed, K.H. Kim, J.-M. Zuo, N. Fang, P. Ferreira, X. Li, Nonlithographic patterning and metal-assisted chemical etching for manufacturing of tunable light-emitting silicon nanowire arrays, Nano Lett. 10 (5) (2010) 1582.
[38] H. Tang, C. Liu, H. He, Surface plasmon enhanced photoluminescence from porous silicon nanowires decorated with gold nanoparticles, RSC Adv. 6 (64) (2016) 59395.
[39] K. Potrick, F. Huisken, Photoluminescence properties of silicon nanocrystals interacting with gold nanoparticles via exciton-plasmon coupling, Phys. Rev. B 91 (12) (2015) 125306.
[40] A. Mooradian, Photoluminescence of metals, Phys. Rev. Lett. 22 (5) (1969) 185.
[41] O.A. Yeshchenko, I.M. Dmitruk, A.A. Alexeenko, M.Y. Losytskyy, A.V. Kotko, A.O. Pinchuk, Size-dependent surface-plasmon-enhanced photoluminescence from silver nanoparticles embedded in silica, Phys. Rev. B 79 (23) (2009) 235438.
[42] P. Gangopadhyay, R. Kesavamoorthy, S. Bera, P. Magudapathy, K.G.M. Nair, B.K. Panigrahi, S.V. Narasimhan, Optical absorption and photoluminescence spectroscopy of the growth of silver nanoparticles, Phys. Rev. Lett. 94 (4) (2005) 047403.
[43] W. Xie, S.-R. Zhang, D.-Y. Du, J.-S. Qin, S.-J. Bao, J. Li, Z.-M. Su, W.-W. He, Q. Fu, Y.-Q. Lan, Stable luminescent metal-organic frameworks as dual-functional materials to encapsulate Ln^{3+} ions for white-light emission and to detect nitroaromatic explosives, Inorg. Chem. 54 (7) (2015) 3290.
[44] Y. Qu, X. Zhong, Y. Li, L. Liao, Y. Huangbc, X. Duan, Photocatalytic properties of porous silicon nanowires, J. Mater. Chem. 20 (2010) 3590.
[45] L. Luo, J. Jie, W. Zhang, Z. He, J. Wang, G. Yuan, W. Zhang, L.C.M. Wu, S.-T. Lee, Silicon nanowire sensors for Hg^{2+} and Cd^{2+} ions, Appl. Phys. Lett. 94 (19) (2009) 193101.
[46] Y. Huang, A.R. Ferhan, S.-J. Cho, H. Lee, D.-H. Kim, Gold nanowire bundles grown radially outward from silicon micropillars, ACS Appl. Mater. Int. 7 (32) (2015) 17582.
[47] C.X. Zhang, L. Liu, H.J. Yin, H. Fang, Y.M. Zhao, C.J. Bi, H.J. Xu, Recyclable surface-enhanced Raman scattering template based on nanoporous gold film/Si nanowire arrays, Appl. Phys. Lett. 105 (1) (2014) 011905.
[48] S.W. Han, S. Lee, J. Hong, E. Jang, T. Lee, W.-G. Koh, Mutiscale substrates based on hydrogel-incorporated silicon nanowires for protein patterning and microarray-based immunoassays, Biosens. Bioelectron. 45 (2013) 129.
[49] H. Wang, L. Mu, G. She, W. Shi, Silicon nanowires-based fluorescent sensor for in situ detection of hydrogen sulfide in extracellular environment, RSC Adv. 5 (81) (2015) 65905.
[50] J. Ghosh, R. Ghosh, P.K. Giri, Tuning the visible photoluminescence in Al doped ZnO thin film and its application in label-free glucose detection, Sens. Actuat. B: Chem. 254 (2018) 681–689.
[51] Y. He, X. Han, D. Chen, L. Kang, W. Jin, R. Qiang, P. Xu, Y. Du, Chemical deposition of Ag nanostructures on polypyrrole films as active SERS substrates, RSC Adv. 4 (14) (2014) 7202.
[52] Y. He, S. Su, T. Xu, Y. Zhong, J.A. Zapien, J. Li, C. Fan, S.-T. Lee, Silicon nanowires-based highly-efficient SERS-active platform for ultrasensitive DNA detection, Nano Today 6 (2) (2011) 122.
[53] M.-L. Zhang, X. Fan, H.-W. Zhou, M.-W. Shao, J.A. Zapien, N.-B. Wong, S.-T. Lee, A high-efficiency surface-enhanced raman scattering substrate based on silicon nanowires array decorated with silver nanoparticles, J. Phys. Chem. C 114 (5) (2010) 1969.